





## Plant-like hooked miniature machines for on-leaf sensing and delivery

Isabella Fiorello <sup>1,2✉</sup>, Fabian Meder <sup>1,3</sup>, Alessio Mondini<sup>1,3</sup>, Edoardo Sinibaldi <sup>1</sup>, Carlo Filippeschi<sup>1</sup>, Omar Tricinci<sup>1</sup> & Barbara Mazzolai <sup>1✉</sup>

New sustainable strategies for preserving plants are crucial for tackling environmental challenges. Bioinspired soft and miniature machines have the potential to operate in forests and agricultural fields by adapting their morphology to plant organs like leaves. However, applications on leaf surfaces are limited due to the fragility and heterogeneity of leaves, and harsh outdoor conditions. Here, we exploit the strong shear-dependent leaf-attachment of the hook-climber *Galium aparine* to create miniature systems that enable precision anchoring to leaf tissues via multifunctional microhooks. We first study the anchoring forces of the microhooks and then fabricate a soft wireless multiparameter sensor to monitor the leaf proximity and degradable hooks for *in-plant* molecular delivery to the vascular tissues of the leaves. In addition, we use a soft robotic proof-of-concept demonstrator to highlight how our hooks enable ratchet-like motion on leaves. This research showcases opportunities for specifically designing multifunctional machines for targeted applications in plant ecosystems.

<sup>1</sup>Bioinspired Soft Robotics Laboratory, Istituto Italiano di Tecnologia, Genoa, Italy. <sup>2</sup>The BioRobotics Institute, Scuola Superiore Sant'Anna, Pontedera, Italy. <sup>3</sup>These authors contributed equally: Fabian Meder, Alessio Mondini. ✉email: [isabella.fiorello@iit.it](mailto:isabella.fiorello@iit.it); [barbara.mazzolai@iit.it](mailto:barbara.mazzolai@iit.it)

To reduce the unsustainable consumption of natural resources and to preserve the health of our planet<sup>1</sup>, natural ecosystems and their complex interrelations need to be fully understood. Plants play an irreplaceable role in this scenario<sup>2,3</sup>, and new sustainable and smart strategies aimed at better understanding their functionalities and to preserve them are becoming more and more important<sup>4–11</sup>. For this reason, there is an increasing interest in using innovative technologies to sense parameters on-site in plants, screen whole plants, and deliver molecules to plants, especially in plant organs for in situ applications<sup>5</sup>. Currently, few devices can directly attach themselves to plant leaves without damaging these leaves due to their fragile and heterogeneous nature. Chemical glue-based<sup>6,11</sup> or clip-based<sup>9</sup> sensors are now being used for the quantitative monitoring of leaf responses to surrounding environmental factors (i.e., water content, temperature, plant growth, and stress). In addition, microneedle-based patches are being developed to penetrate leaves in order to deliver the payload to plant tissues<sup>7</sup> and to rapidly detect plant diseases<sup>8</sup>.

Living organisms can inspire scientists in the prototyping of bioinspired soft machines able to operate in dynamic real-world environments<sup>12–16</sup> to tackle environmental-related issues<sup>17,18</sup>. When miniaturized, these machines can noninvasively and precisely access confined spaces<sup>19,20</sup>. Although the use of such machines in natural habitats is restricted, they may lead to a disruptive robotic vision where they can adapt to dense vegetation, such as on plant leaf organs, to closely monitor and preserve natural ecosystems, thus reducing the use of potential pollutants<sup>21</sup>.

Plants have evolved to colonize several habitats by exploiting different types of permanent or reversible anchoring strategies to attach themselves to the surrounding vegetation, rocks, barks, trees, or animals<sup>22–29</sup> (for a brief overview of the main anchoring strategies in plants see Supplementary Table 1). One of the main reversible anchoring strategies in plants exploits hook-like structures (e.g., spines<sup>25</sup>, prickles<sup>25</sup>, microhooks<sup>22</sup>, and burrs<sup>26,30</sup>), of different shapes and sizes depending on the species (Supplementary Fig. 1). In particular, the hook-climber *Galium aparine* uses a unique parasitic ratchet-like anchoring mechanism to climb over host plants using microscopic hooks for mechanical interlocking to leaves<sup>22,31</sup>.

Using a high-resolution additive manufacturing technique<sup>32</sup>, we recently proposed the climbing mechanism of *G. aparine*<sup>22</sup> as a competitive strategy to attach to textiles and skin tissues<sup>33</sup>, which showed encouraging results for the biomedical and clothing industries.

Here, we advanced such plant-like miniature adhesive systems to enable exceptional soft machine-leaf interactions by a multifunctional directional anchoring through microhooks (MH) to various plant leaf surfaces for in situ leaf microenvironment monitoring and molecular delivery to plant vascular tissues.

First, we built flexible and optionally degradable MH-based devices at high resolution using two-photon lithography directly or combined with micromoulding and casting of different materials. Second, we characterized the morphological and biomechanical features of different leaf surfaces and the attachment performances of the MH-based devices to different leaves in order to define the mechanical dynamics involved, such as correlating the influence of plant leaf epidermal microstructures, roughness, and hardness to their attachment behavior. Third, we exploited MH-based flexible leaf-attachment systems in miniaturized and customized origami-assembled multiparameter leaf sensors for leaf microclimate monitoring. Fourth, we used MH-based self-dissolving systems for the localized release of molecules on a leaf, producing biodegradable environmental-friendly machines. Finally, we introduced a proof-of-concept demonstrator based on

the *Galium aparine*-inspired hooks that enables ratchet-like motion via the repeated engagement/disengagement of the hooks to leaf tissues. This dynamic anchoring system could be interesting for motion scenarios in unstructured environments such as leaf surfaces.

We highlight how a plant-like anchoring strategy via microhooks can be used for attaching to, moving on, and penetrating plant leaf tissues to closely sense the leaf's microclimate or deliver small amounts of molecules. Our findings advance the vision of fully integrated plant-inspired multifunctional miniature machines that may in the future operate in ecosystems to protect and preserve plants and biodiversity<sup>21</sup>.

## Results and discussion

**Concept and prototyping.** Field observations of *G. aparine* show its capacity to move over diverse host plant species, anchoring via microscopic hooks on its abaxial leaf side, which mechanically interlock, like ratchets, with the host leaf (Supplementary Fig. 2)<sup>22</sup>. Microscope observations show that abaxial hooks have a unique downward orientation (Fig. 1a)<sup>22</sup>, which enables them not only to anchor but also to penetrate leaf surfaces (Fig. 1b, c).

We thus designed and modelled *G. aparine*-like artificial abaxial hooks as described in detail in ref. <sup>33</sup> to create two different types of devices with patterned artificial abaxial microhooks capable of directional attachment on leaves, including flexible IPS-made MH-based devices (IPS-MHDs) and self-dissolving isomalt@fluorescein MH-based devices (i@fluo-MHDs) (Fig. 1d–f, Supplementary Figs. 3–6). The design and geometrical details of artificial hooks are reported in Supplementary Fig. 3 and Supplementary Tables 2 and 3.

IPS-MHDs are microfabricated at a high resolution and high reproducibility using two-photon lithography (Nanoscribe Photonic Professional system) on flexible polyethylene terephthalate (PET) sheet substrates with the photoresist IPS (Fig. 1e, Supplementary Fig. 4a, part A; see Methods for details)<sup>33</sup>. On the other hand, i@fluo-MHDs are microfabricated by strategically combining two-photon lithography with micromoulding of biodegradable materials (Fig. 1f).

Briefly, a hook pattern made using a photoresist on a silicon wafer was used to create a PDMS mould. This thus enabled the high-throughput fabrication<sup>34,35</sup> of self-dissolving hooks using natural polymers such as isomalt as a matrix for in-plant delivery of molecules (Supplementary Fig. 4a, part B and 4b–l, Supplementary Fig. 5). Water-dissolvable materials are often used to make microneedle-based patches, including diverse hydrogels<sup>8,34</sup> and silk fibroin based-biomaterials<sup>7</sup>. However, the toughness of hydrogel materials is insufficient to penetrate leaf surfaces in shear direction and microhook confirmation (Supplementary Fig. 6a).

Here we propose isomalt, a low-cost, nontoxic, recyclable sugar substitute with unique toughness properties<sup>36</sup>, which enables the fabrication of strong, water-dissolvable hooks capable of anchoring and penetrating leaves in shear direction (Fig. 1f, right side).

Figure 1g and Supplementary Movie 1 illustrate the proposed concept for directional attachment on plant leaves, also comparing the attachment behavior between *G. aparine* natural and artificial hooks (Supplementary Movie 1).

**Structural and mechanical characterization.** To investigate the adhesive behavior of MHDs on plant surfaces and correlate the influence of structural and mechanical leaf properties<sup>37,38</sup> on hook attachment, we performed normal and shear attachment experiments on fresh leaves with varied epidermal microstructuring (i.e., increasing cell shape and size, presence of hairs), roughness, and tissue hardness (Fig. 2). To the best of our knowledge, this is the first exploitation of artificial hooks for

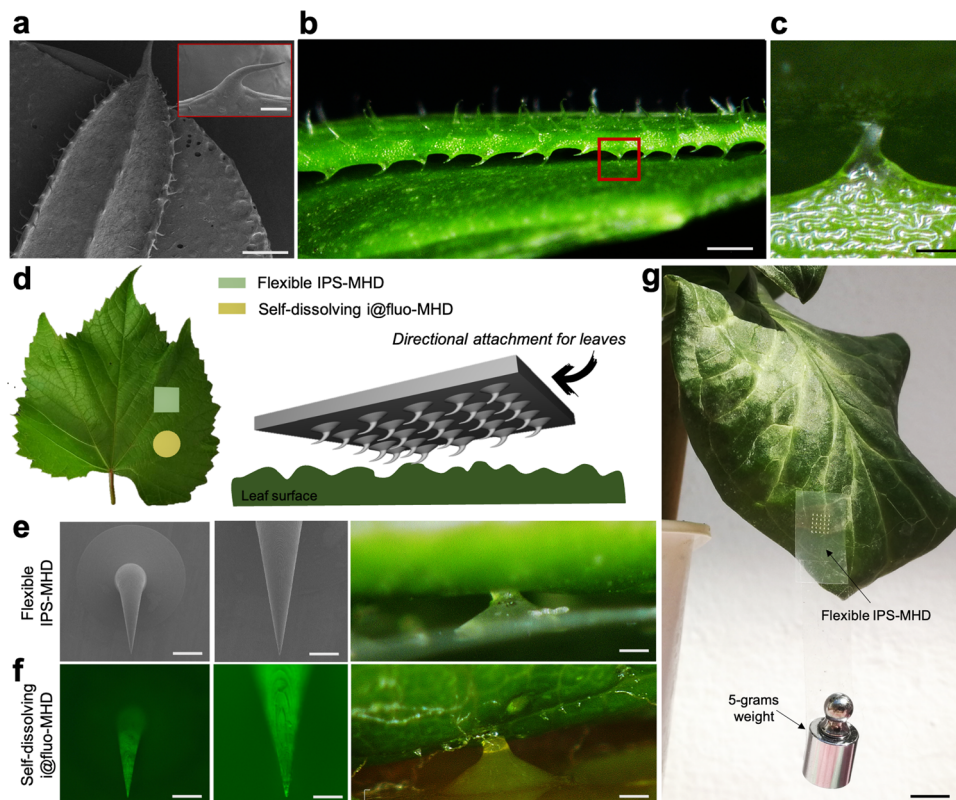


**Fig. 1** From natural to artificial MH-based anchoring devices for plant leaves. **a** SEM images of *G. aparine* natural abaxial leaf side (scale bar, 1 mm) and close up of natural abaxial microhook (inset, scale bar, 150  $\mu\text{m}$ ). **b, c** Digital microscope images of *G. aparine* leaf on a host plant (scale bar, 500  $\mu\text{m}$ ) and focus on natural abaxial microhook interlocking with the leaf surface (scale bar, 200  $\mu\text{m}$ ), respectively. **d** MH-based directional attachment system on leaves. **e** Artificial hooks of flexible IPS-made MH-based devices (IPS-MHDs) and their interlocking with leaf surface (SEM images on the left). Scale bars, 100 and 25  $\mu\text{m}$ , respectively; digital microscope image on the right, scale bar, 100  $\mu\text{m}$ . **f** Artificial hooks of self-dissolving isomalt@fluorescein-made MH-based devices (i@fluo-MHDs) and their interlocking with leaf surface (fluorescence images on left). Scale bars, 200 and 50  $\mu\text{m}$ , respectively; digital microscope image on right, scale bar, 200  $\mu\text{m}$ . **g** Demonstration of directional attachment on *Arum italicum* leaves using IPS-MHDs (i.e., holding a weight of 5-grams). Scale bar: 1 cm.

shear-direction-dependent reversible attachment to natural plant leaves.

First we classified the leaves based on their epidermal structure and roughness<sup>37,39</sup> using SEM and an optical profilometer<sup>39–41</sup>. Leaves were subdivided into: (1) smooth leaf surfaces (as the control), which consisted of flat tabular cells (i.e., young (MY) or mature (MM) leaves of *Magnolia grandiflora*); and (2) rough surfaces, which consisted of convex cells, with or without hairs (Fig. 2a).

To describe rough surfaces without hairs, we identified four categories with increasing convex cell dimensions (i.e., adaxial leaf sides of *Hedera helix* (HH), *Arum italicum* (AI), *Vitis vinifera* (VV), and *Vitis lambrusca* (VL<sub>AD</sub>)). To describe rough surfaces with hairs, we identified three categories according to hair densities or shape (i.e., short erect hairs with low density: adaxial side, *Rubus caesius* (RC<sub>AD</sub>); short erect hairs with high density: abaxial side, *Rubus caesius* (RC<sub>AB</sub>); long helicoidal hairs: abaxial side, *Vitis lambrusca*, VL<sub>AB</sub>) (Fig. 2a).

As illustrated in Fig. 2b, the average roughness ( $S_a$ ) of the leaves significantly increased from smooth to rough leaf surfaces without hairs (i.e., from  $3.7 \pm 0.3 \mu\text{m}$  to  $11.8 \pm 2.5 \mu\text{m}$ ,  $\times 10$ ), reaching the maximum  $S_a$  on high-density helicoidal hairy surfaces (i.e.,  $37.3 \pm 5.2 \mu\text{m}$ ,  $\times 10$ ). Supplementary Fig. 7a report the  $S_a$  at  $\times 50$  magnification. Using a dynamic nanoindentation system<sup>42–44</sup>, we then characterized the average hardness ( $E$ ) of small leaf tissue volumes<sup>38</sup> at 1–200 Hz, and observed that leaves collected from *G. aparine* host plants have  $E$  up to  $17.6 \pm 4 \text{ MPa}$

(Supplementary Fig. 8). As a control, we also measured the  $E$  of smooth stiff surfaces, such as mature ( $E$  up to  $128 \pm 43 \text{ MPa}$ ) and young leaves ( $E$  up to  $73 \pm 18 \text{ MPa}$ ) of *M. grandiflora* (Supplementary Fig. 8).

Overall, the results of the pull-off, shear locking and friction force tests on flexible IPS-MHDs showed that artificial hook attachment was strongly influenced by structural and mechanical leaf features (Fig. 2c–e, Supplementary Figs. 7, 8).

In a typical pull-off and shear-locking force test<sup>33</sup>, a fixed preload is applied to ensure the proper overlap between the two tested surfaces, with hooks penetrating leaf tissues. The higher detachment strength of hooks ranged from  $0.6 \pm 0.2 \text{ N cm}^{-2}$  on smooth surfaces to  $1.1 \pm 0.2 \text{ N cm}^{-2}$  on rough surfaces without hairs, reaching a maximum of  $1.3 \pm 0.4 \text{ N cm}^{-2}$  on rough surfaces with helicoidal hairs (Fig. 2c). High direction-dependent shear-locking forces were generated from IPS-MHDs over fresh smooth ( $5.9 \pm 1.4 \text{ N cm}^{-2}$ ) and rough surfaces (up to  $10.4 \pm 2.0 \text{ N cm}^{-2}$  on rough surfaces with helicoidal hairs). Lower forces were observed when using a lower preload of 0.05 N, likely due to a reduced hook penetration and/or a reduced number of hooks effectively engaging with leaf tissue (Supplementary Figs. 7, 9) (e.g., as occurs for other soft tissues like skin<sup>33</sup>). In addition, below a certain preload threshold, for example at 0.02 N, negligible detachment forces were obtained (Supplementary Fig. 9a).

The pull-off and shear-locking performances of IPS-MHDs on leaves depend not only on leaf microstructuring, but also on the



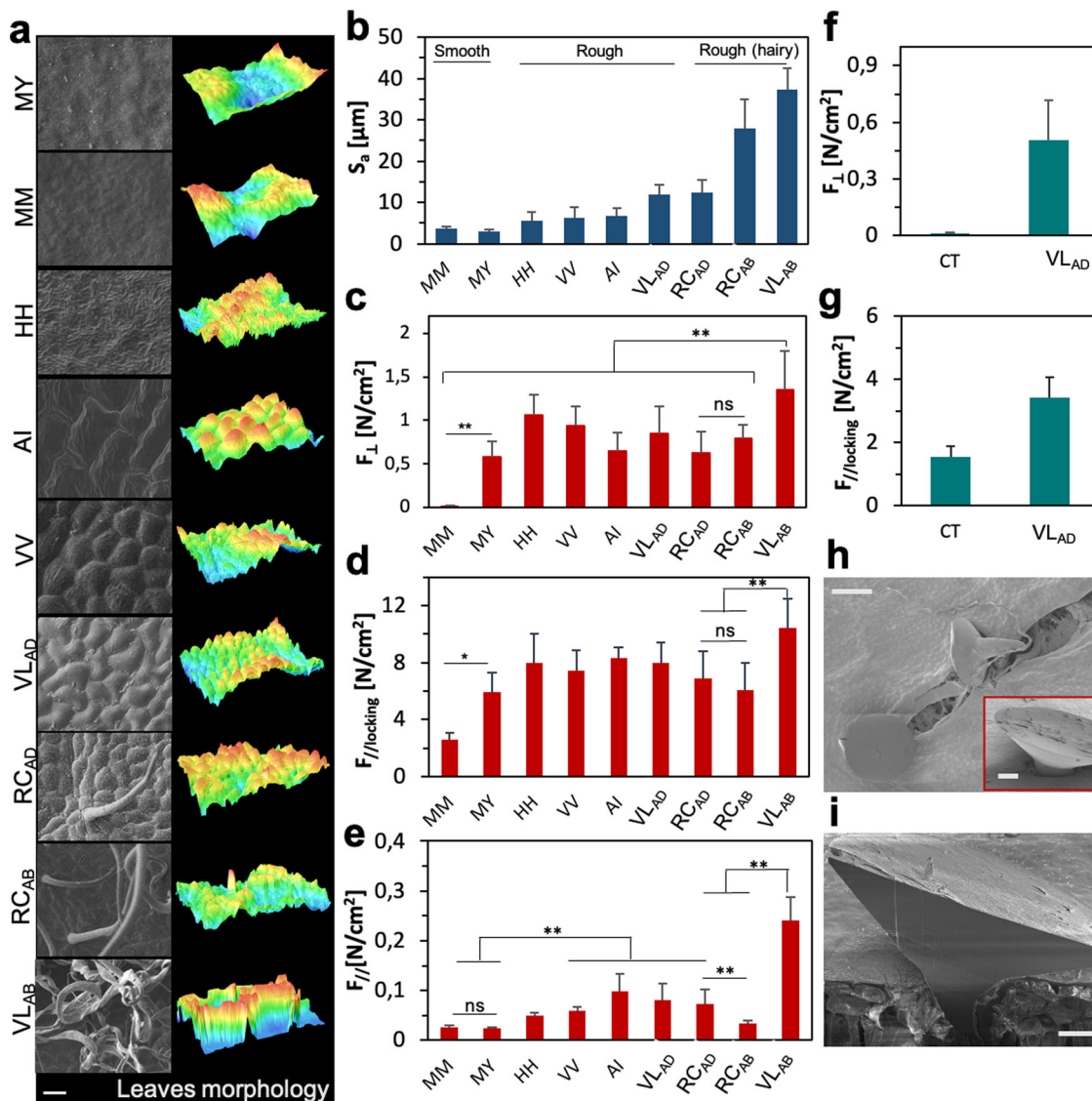


**Fig. 2 Structural and mechanical characterization of leaf surfaces and hook interaction.** **a** SEM images (left) and 3D profilometry (right) of leaf surfaces of typical *G. aparine* host species, including *M. grandiflora* (young and mature smooth adaxial leaf surfaces, MY and MM, respectively), *Hedera helix* (rough adaxial leaf surfaces, HH), *Arum italicum* (rough adaxial leaf surfaces, AI), *Vitis vinifera* (rough adaxial leaf surfaces, VV), *Vitis lambrusca* (rough adaxial leaf surfaces, VL<sub>AD</sub>), *Rubus caesius* (rough adaxial leaf surfaces with low-density erect hairs, RC<sub>AD</sub>), *Rubus caesius* (rough abaxial leaf surfaces with high-density erect hairs, RC<sub>AB</sub>), and *Vitis lambrusca* (rough abaxial leaf surfaces with helicoidal hairs, VL<sub>AB</sub>). Scale bars, 20 μm. **b** Average roughness ( $S_a$ ) of the tested leaf surfaces at  $\times 10$  magnification. **c, d** Maximum pull-off forces ( $F_{\perp}$ ) (**c**) and maximal shear-locking forces ( $F_{//locking}$ ) (**d**) at 1 N preload generated by IPS-MHDs in the interlocking direction on the different tested leaves. The asterisks indicate statistical significance with  $p$ -value  $> 0.05$  (ns),  $p$ -value  $< 0.05$  (\*), or  $p$ -value  $< 0.01$  (\*\*) (analysis of variance with ANOVA followed from post-hoc Tukey's test). **e** Friction forces generated by the IPS-MHDs pulled in the direction of hook tip on the various leaves tested. The asterisks indicate statistical significance with  $p$ -value  $> 0.05$  (ns) or  $p$ -value  $< 0.01$  (\*\*) (ANOVA followed by post-hoc Tukey's test). **f, g** Maximum pull-off forces (**f**) and maximal shear-locking forces (**g**) generated by i@fluo-MHDs in the interlocking direction over the adaxial side of *V. lambrusca* leaf. As a control, a device without hooks was tested (CT). **h** SEM images of hooks after shear-locking attachment tests over MY leaf. Scale bar, 200 μm. Inset: Hook penetration inside leaf. Scale bar, 50 μm. All error bars report the standard deviations. **i** Cross view using FIB-SEM of a microhook anchoring and penetrating young MY leaf. Scale bar, 100 μm.

leaf hardness. The developed hooks were able to attach themselves onto the entire fresh leaf surfaces with  $E$  up to  $73 \pm 18$  MPa (Fig. 2c–e, Fig. 2h–i). However, hooks were unable to attach onto MM ( $E$  up to  $128 \pm 43$  MPa, Supplementary Fig. 8), as the tissue was too stiff for the hooks to penetrate (Fig. 2c, d).

Unlike for the pull-off and shear-locking tests<sup>33</sup>, the frictional properties of flexible IPS-MHDs on leaves were investigated using a similar protocol used for *G. aparine* natural leaves<sup>22</sup> (Fig. 2e), where no fixed preload was applied and hooks interlocked only “temporarily” onto the surface, without penetrating the leaf tissue. Our results show that increasing friction forces were generated

when IPS-MHDs were pulled over leaf surfaces in correlation with the roughness of the leaf (Fig. 2b, Supplementary Fig. 7a), except for high-density erect hairs, which negatively affect the friction forces of hooks (Fig. 2e).

Although the presence of high-density erect hairs did not influence the shear-locking forces (Fig. 2d), in friction tests, erect hairs may act as a “screen” on the leaf tissue, due to the lack of a proper preload to achieve leaf penetration (Fig. 2e). In contrast, the presence of helicoidal hairs may like a Velcro loop on the leaf surface, and the hooks can strongly interlock onto the hairs, thus significantly increasing the friction forces up to  $0.24 \pm 0.05$  N cm<sup>-2</sup>

(Fig. 2e). Typical force-displacement curves obtained from shear-induced attachment experiments are reported in Supplementary Fig. 10.

Figure 2f and g shows the pull-off and shear-locking forces of self-dissolving i@fluo-MHDs tested on the adaxial side of *Vitis lambrusca* leaves. The devices showed a maximum detachment force of  $0.5 \pm 0.2 \text{ N cm}^{-2}$  and a maximum shear-locking force of  $3.4 \pm 0.6 \text{ N cm}^{-2}$ , thus demonstrating their potential for work on plant leaf surfaces.

Finally, we investigated the effect of hooks density and size on leaf attachment (Supplementary Figs. 11, 12; for geometrical details see Supplementary Tables 2, 3). With regard to the density of the hooks, based on a reference value ( $156 \text{ hooks cm}^{-2}$ , associated with a  $5 \times 5$  MH array), we considered both lower ( $49 \text{ hooks cm}^{-2}$ ,  $3 \times 3$  MH array) and higher ( $352 \text{ hooks cm}^{-2}$ ,  $7 \times 7$  MH array) densities. Relatively weaker attachments were observed when both reducing and increasing the number of hooks for the reference surface for a given preload (Supplementary Fig. 11d, e). Force reduction appeared to be consistent with a corresponding reduction in the number of hooks, as expected due to the lower number of hooks that engaged in contact with the leaf surface. On the other hand, in order to investigate force reduction at higher densities, we introduced a 3D computational model (Supplementary Fig. 13a), by focusing on the vertical force associated with pull-off.

In view of model objective and constraints, including data availability for calibration, we first considered the initial MH extraction, i.e., small vertical displacement from the initial, embedded configuration. The numerical results highlighted a very local hook-leaf biomechanical interaction (Supplementary Fig. 13b), due to the strong differences in stiffness among the materials involved. We thus focused on the effects of the density of the hooks in the previous penetration phase. To do this we introduced a simplified 2D penetration model (Supplementary Fig. 13c). This model shows that as spine density increases for a given preload, penetration could be hampered more than proportionally to the number of spines. Consequently, the subsequent extraction (i.e., pull-off) of the whole spine array was achieved by applying a reduced force. This result, which is in agreement with the aforementioned experimental findings (Supplementary Fig. 11d), can be explained by observing how the density of hooks can increasingly affect hook-leaf interaction on a relatively less local length. Higher densities also compress the upper epidermal surface of the leaf, which in turn further hampers penetration (Supplementary Fig. 13c).

With regard to the effects of the size of the hooks, we observed that down-scaled (0.5:1) MH failed to engage with leaf tissues, whereas upscaled (2:1) ones enabled leaf anchoring and showed comparable attachment forces with respect to the original (1:1) MHs (Supplementary Fig. 12d, e). Using our 3D computational model, we also investigated the effect of MH upscaling on leaf attachment. We found that the initial extraction force increases less than proportionally with respect to hook size (Supplementary Fig. 13d). The strong difference in stiffness between MH and leaf tissue materials seems to play a role in the moderate effect of size. However, we cannot make strong quantitative claims in this regard. For instance, an increase in hook size may introduce complex effects both in the initial penetrating phase and any fractures at pull-off. This is also due to the relatively more important geometrical interface conditions with the upper epidermis, which has an important role due to the relatively stiffer character compared to mesophyll<sup>45–47</sup>.

More ambitious claims could be made, for instance based on a wider set of biological data, which are currently not available in the literature. In addition, the simplifications needed to model the MH-leaf system intrinsically have some limitations. In particular,

we were unable to address the spatial distribution of effective hook-tissue engagement. In fact, symmetry-breaking effects due to local tissue heterogeneity, and load distribution effects amongst hooks in an array (based on specific working conditions, i.e., precision leaf applications), add to the complexity of the problem. Hence, also in view of possible specific applications, future work could investigate how the load is shared between arrays of hooks in a variety of plant tissues, for example similarly to load-sharing previous studies performed across a multiplicity of spines<sup>48</sup>, or hooked-like mushrooms<sup>49</sup>.

Although some studies have investigated the influence of leaf structures on the attachment of natural organisms (e.g., insects)<sup>39</sup>, we believe that our study is the first to investigate the influence of leaf properties on artificial devices for precision leaf attachment. In addition, although a few other artificial strategies (e.g., microneedle-based patches)<sup>7,8</sup> have been developed for leaf tissue interlocking, our strategy using microhooks exhibits the highest available shear-dependent anchoring to leaf tissues of up to  $10.4 \pm 2.0 \text{ N cm}^{-2}$ . In addition, the particular shape of our hooks allows in situ reversible attachment to leaves simply by changing the direction of the applied load, thus no relevant additional force is required to disengage the device from the leaves. In fact, shear-direction-dependent engagement/disengagement is an important feature for engineering and robotics. In addition, our hooks, which employ shear-dependent interlocking onto leaves with two different materials (IPS resist or isomalt), show multifunctionality for several small-scale on-leaf applications.

**Environmental MH-based machines.** To explore the use of MHDs for real-world in situ leaf applications, we designed and built three different machines (Figs. 3 and 4).

The first demonstration machine is a MH-based miniaturized wireless multiparameter origami-assembled device for leaf microclimate monitoring (Fig. 3a–c). There has been increasing interest in robotics and engineering fields in designing architected materials based on origami, by folding two dimensional structures (e.g., sheets) into three-dimensional components<sup>50,51</sup>. Here we exploit an origami-like strategy to facilitate the assembly of light-weight microdevices consisting of a single flexible PET sheet with directly aligned microprinted IPS hooks (Fig. 3a, Supplementary Fig. 14a–c). We combined it with the use of flexible PCB containing multiple sensors in a custom-made configuration (Fig. 3a, Supplementary Fig. 14a, d). The sensing mechanism is based on commercial low-cost digital capacitive-type humidity sensor and a bandgap temperature sensor connected by a I2C communication channel to the Bluetooth microcontroller. For clarity, the characteristics of the sensors (including the type of sensor, resolution, accuracy, sensitivity, and working range) are summarized in Supplementary Table 4. Thanks to our microhooks and the origami-assembled approach, we obtained a unique three-dimensional foldable multifunctional fully integrated device, which can simultaneously monitor crucial parameters of both the upper and lower leaf sides (Fig. 3a), including temperature, light, and humidity. These parameters strongly affect plant health, productivity, and growth<sup>6,10</sup> and can be used as input (e.g., response to hydration parameter changes nearby the leaves) to understand when to start irrigation (thus reducing water consumption) or to predict the possible occurrence of pathogens (using pesticides only when necessary, and thus with less pollution).

As expected from the adhesive experiments (Fig. 2d), the device (weighing 2.36 g) strongly attaches itself to plant leaves when directionally interlocked onto the leaf (Fig. 3b). It can also be reused for several leaves simply by attaching and detaching it from their surface by turning the direction of the applied load (Supplementary Movie 2).

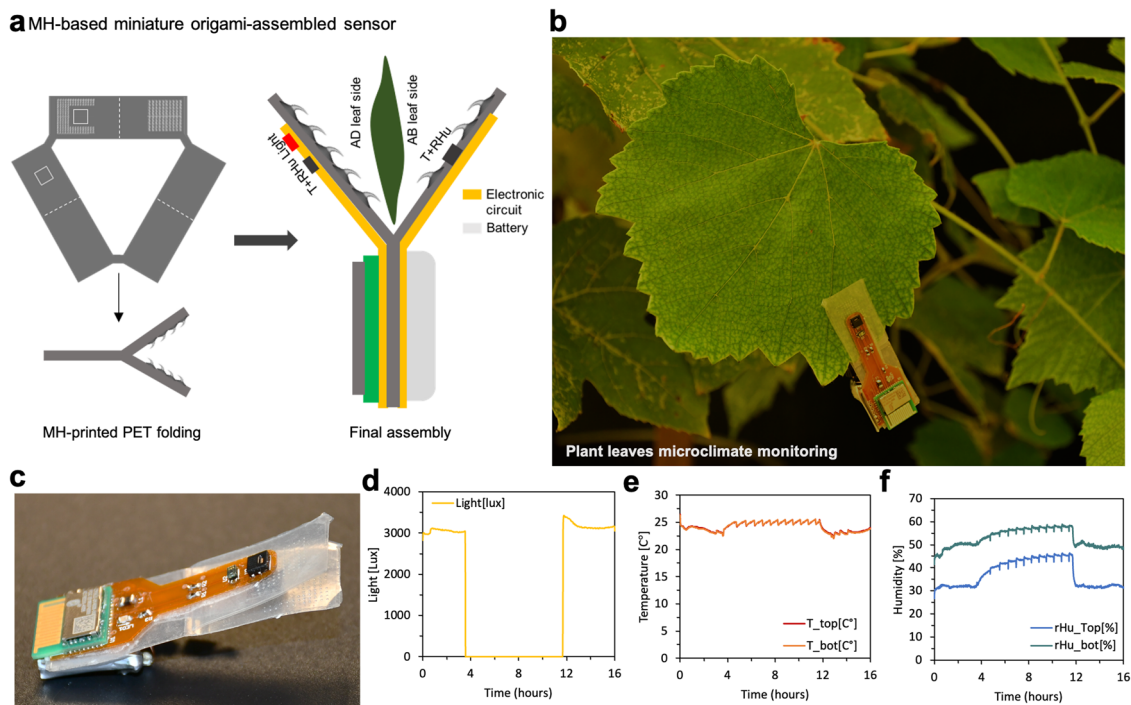


**Fig. 3 Environmental machines made with flexible IPS-MHDs.** **a** A fully integrated origami-assembled device embedding microprinted hooks, electronic circuit, sensors, and battery. **b, c** Pictures of MH-based sensor for leaf microclimate monitoring. **d–f** Plotting results of light, temperature, and humidity parameter monitoring of *V. lambrusca* leaves in growth chamber conditions over 16 h. Temperature and humidity parameters are reported for both adaxial and abaxial *V. lambrusca* leaf sides.

The data acquired are transmitted wirelessly with a customized software to a computer. Plots of light, temperature, and humidity vs time are reported in Fig. 3d–f, respectively, which show the real-time monitoring of *Vitis lambrusca* leaves, a typical grapevine cultivated in vineyards. The device shows its potential for use also in outdoor conditions, demonstrating its strong attachment and resistance to windy conditions (Supplementary Fig. 14e–g, Supplementary Movie 2), and for real-time measurements for up to 50 days (Supplementary Fig. 14h).

Overall, our device shows great potential for practical use for both small-scale and large-scale applications. For small-scale applications, researchers can use it to accurately monitor localized portions of each tested plant, which is crucial for physiological and botanical studies. For large-scale applications, farmers can distribute many of these devices in order to map wide cultivation areas for industrial applications.

In addition, MH structures may be used to deliver molecules directly to the leaf tissue in a similar way to a drug-delivery vehicle, as they can directionally penetrate leaf tissue and rapidly dissolve inside the plant sap to inject a small amount of chemicals (Fig. 4a–d, Supplementary Fig. 15a, Supplementary Movies 3 and 4).

Isomalt-made MH have a high potential for use as plant-like tools for the precise release, similarly to silk fibroin-microneedle patches<sup>7</sup>, of fungicide/bactericides, micro/nanoparticles<sup>5,52,53</sup> or other molecules to leaf tissues by being directly released through the hook array (Fig. 4e–h). Our plant-inspired approach also enables reversible attachment, direction-based locomotion and sensing to leaves by the same structure. The isomalt matrix is particularly suitable for (i) loading the cargo<sup>54</sup>; (ii) creating microhooks of sufficient mechanical stability that penetrate the tissue in a straightforward, upscalable process; and (iii) dissolving in the inner leaf tissue to release the cargo. It is also cheap, widely available, and environmentally safe. Moreover, the use of sugar alcohols like isomalt in plants seems promising due to the lack of toxicity and the even protective effect against photooxidative

stress<sup>55</sup>. Hook injection and isomalt degradation caused no evident adverse reaction to plant health in the short term (up to several days after injection) despite a very local scar tissue, self-healed by the plant, where the hooks penetrated the tissue but there was neither effect on the viability of the leaf nor the plant (Supplementary Fig. 16). However, further studies are necessary to investigate plant responses to the injection of isomalt-made hooks in the long term (e.g., through  $\text{Ca}^{2+}$  signaling<sup>56</sup>). Future work could also identify the most suitable cargos for encapsulation in the isomalt matrix (e.g., sulfur ions such as fungicide/bactericides, micro/nanomaterials)<sup>5,52,53</sup> and how they affect plant health.

After directionally shear-induced injecting the self-dissolving i@fluo-MHDs onto *V. lambrusca* leaves, we recorded the small molecule delivery and mobility through the vascular tissue using a fluorescein-loaded isomalt matrix (Fig. 4e–h, Supplementary Movie 5). We noted a distinct time-dependent decrease in the fluorescence intensity at the penetration site of the hooks (Fig. 4e, f, Circles 1 and 2, Supplementary Movie 5). On the other hand, there was a time-dependent increase in fluorescence intensity in plant vascular tissues “far” from the injection site (Fig. 4e, g–h; Circles 3 and 4, 5, and 6, Supplementary Movie 5), suggesting that isomalt@fluorescein material is absorbed, which dissolved in the plant sap and released the fluorescence which is eventually transported to the vascular tissue (e.g., phloem). We demonstrated the fast dissolution of i@fluo-MHDs in vitro in water at room temperature, showing complete dissolution in less than 10 min (Supplementary Fig. 15b, Supplementary Movie 6). We also recorded in real-time the response to environmental humidity and direct water exposure of the single hook level (Supplementary Movie 7). The tip of the hook dissolves rapidly when directly exposed to bulk water and it dissolves completely in about 10 seconds, Fig. 4i. This suggests that there is a fast molecular delivery in the plant sap. The hook is fully biodegradable<sup>36</sup> and dissolves more slowly in natural environments.



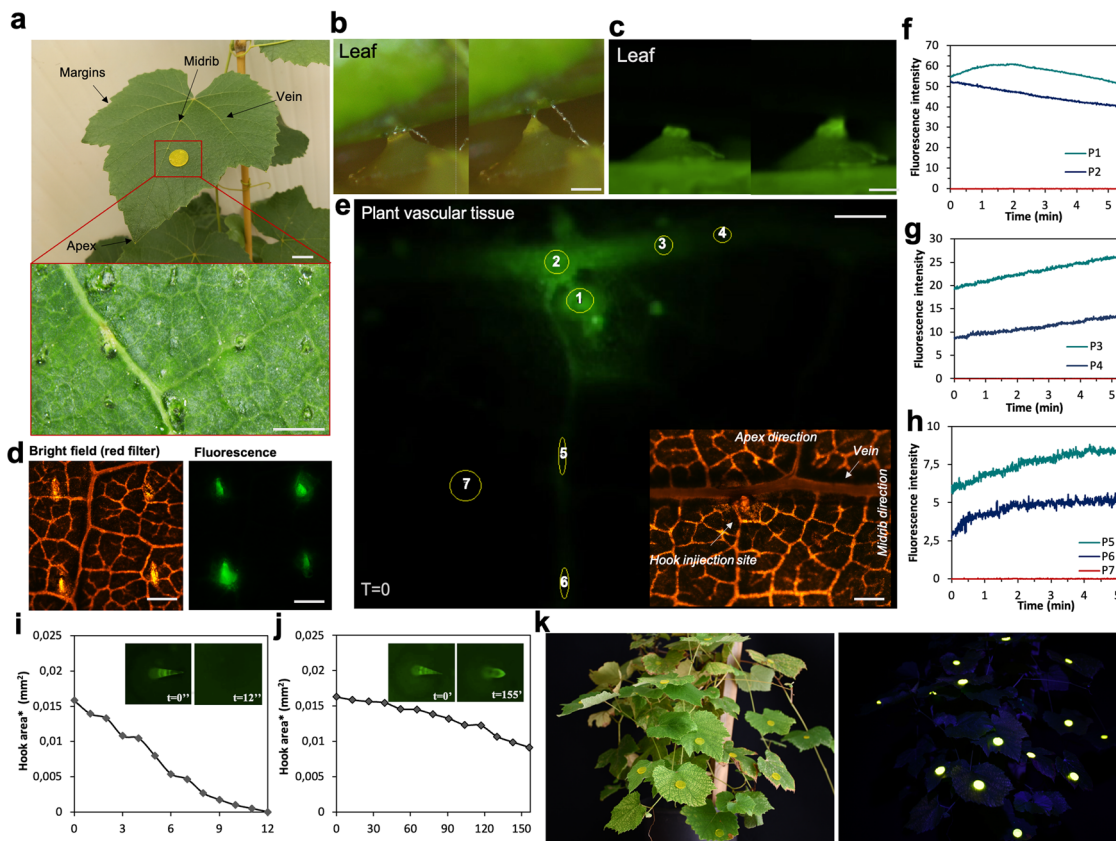


**Fig. 4 Precision plant delivery based on i@fluo-MHDs.** **a** Example of an i@fluo-MHD attached to a leaf. For clarity, the main leaf parts (e.g., margins, apex, midrib, and veins) are indicated. Scale bar, 1 cm. In the inset, a digital microscopy view of the leaf injected site is reported. Scale bar, 1 mm. **b, c** Digital (**b**) and fluorescence (**c**) microscopy images of single hook dissolution after interlocking to a *V. lambrusca* leaf. Scale bars, 500  $\mu\text{m}$ . **d** Bright field microscopy images with a red filter (right side) and fluorescence (left side) images of areas of the leaf injected via hook arrays. Scale bars, 500  $\mu\text{m}$ . **e** Fluorescence images of plant veins after removing the i@fluo-MHDs from the leaf of *Vitis lambrusca*. The i@fluo-MHD was positioned near the midrib (similarly to panel **a**) and a vein was penetrated. The circles and ellipses indicate the investigated area on the vascular tissues. Scale bars, 300  $\mu\text{m}$ . Inset: bright field image showing orientation of the injection site with respect to the leaf. Scale bar, 500  $\mu\text{m}$ . **f-h** Fluorescence intensity variation over time in the vascular plant tissue at the corresponding numbered circle indicated in panels **e, i, j**) Variation of hook area versus time during dissolution in **i** immersion in water and **j** ambient humidity. In particular, hooks area\* represents the projected area of the hook extracted from 2D fluorescence images (from Supplementary Movies 7). Insets: Fluorescence microscopy images of the individual hook before and after degradation for both conditions. **k** Proof-of-concept pictures of many miniature MH-based dissolvable machines scattered over a grapevine leaf for plant preservation under white light (left) and UV illumination (right).

In fact, as a response to environmental humidity, the hook tips partially dissolve in about 150 min (Fig. 4j). As single hooks already partially dissolve under environmental humidity, if longer preservation is needed, a thin protective layer that delays dissolution can be applied (i.e., silk fibroin) on the hooks.

These results suggest that dissolvable machines could be used as a plant-inspired tool for *in situ* delivery in plants. These machines could be applied on several plant leaves (proof-of-concept pictures in Fig. 4k) to deliver their molecular payload.

Finally, direction-based hook-shaped microstructures not only enable static anchoring and penetration of the tissue, but can also be used for dynamic reversible anchoring via repeated engagements of the hooks with and disengagement from the leaf. Dynamic reversible anchoring has been demonstrated in specifically designed robots<sup>57–61</sup>. For example, ratchet-like actuation via insect-like microspines was exploited in SpinyBot<sup>59</sup> for climbing concrete and rocks surfaces (i.e., where the surface is rigid), and in CLASH<sup>58</sup> robots to climb up loose suspended cloth surfaces (i.e., surface rigidity is not guaranteed).

Here, we show that the *Galium aparine* microhooks can enable a ratchet-like attachment/detachment on complex unstructured surfaces such as leaves (a proof-of-concept prototype is shown in

Fig. 5a). To illustrate dynamic reversible anchoring on leaves, we integrated our MHs structures into a low, insect-like, 190 mg demonstrator enabling forward locomotion on leaf tissues (i.e., MH-based MiniBot, Fig. 5a, b). The robot is made of PET with directly printed IPS microhooks oriented as described in Supplementary Fig. 17a. The structure is actuated by a soft fluidic multiphase actuator that can be remotely driven by on-off cycling of a near-infrared laser (808 nm, ~250 mW) (Fig. 5b, Supplementary Fig. 17) as previously described in<sup>62</sup>. We tested the directional locomotion of the MH-based MiniBot on a leaf with and without a small weight (0.036 g), using a dedicated setup with a laser, a thermo camera and a video camera (Supplementary Fig. 17b–d, Supplementary Movie 8). Upon multicycle actuation, the MH-generated forces (i.e., without the need of additional preload) enable MiniBot forward motion.

To the best of our knowledge, this is the first proof-of-concept plant-inspired machine capable of ratchet-like dynamic reversible anchoring over a leaf. This soft machine was introduced purely for demonstration purposes. Indeed, many technical challenges still need to be solved before plant-inspired miniature robots may work in extremely unstructured environments such as natural fields, in dense vegetation, and also resisting wind, rain,

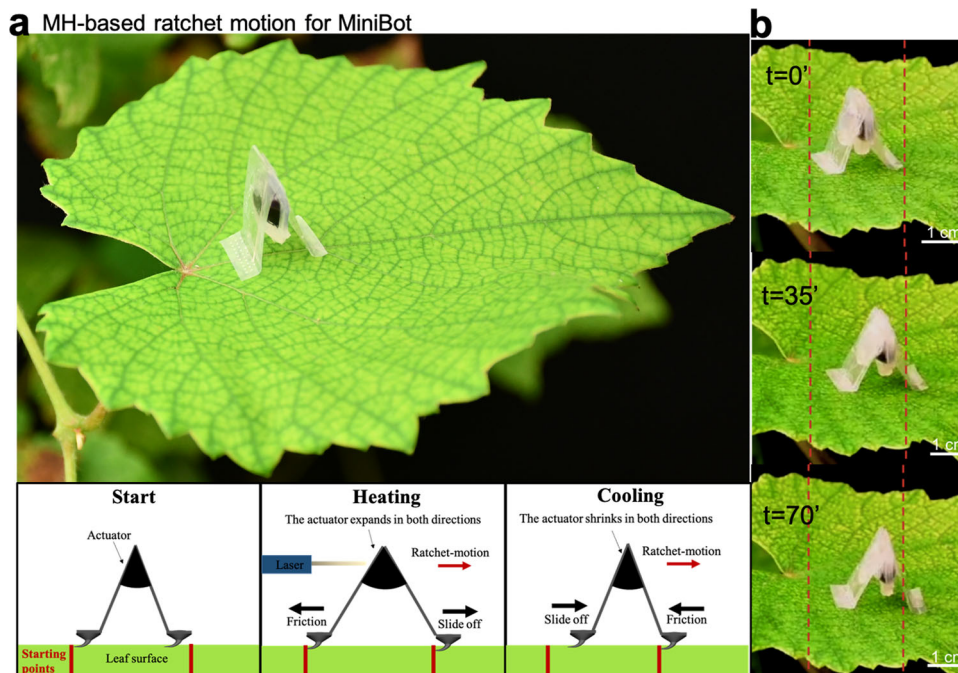


**Fig. 5 Proof-of-concept demonstrator of ratchet-like motion on leaf surfaces via MH structures embedded in a miniature robot (MH-based MiniBot).** **a** MH-based MiniBot over a *V. lambrusca* leaf. Inset: the interlocking mechanism enabled by the MH printed on the feet of the light-driven, low-weight MiniBot. When the 808 nm laser hits the actuator, the actuator expands and the MHs on the back foot create friction with the leaf surface. At the same time, the hooks on the front foot slide off enabling the demonstrator to move forward, and blocking backward motion. During the laser-off phase, when the fluidic actuator cools down it shrinks. The MHs of the front foot then interlock and/or create sufficient friction to remain in the position obtained during expansion of the actuator, whereas the hooks on the back foot slide forwards, enabling on-leaf mobility of the robot. **b** Single frames at different timepoints showing the forward motion of MH-based MiniBot on the *V. lambrusca* leaf.

temperature variations etc. These issues could be solved by overcoming challenges in micro-manufacturing, sensing, actuation, power, and control<sup>63</sup>. Future work could focus on the design of small mobile or aerial robots<sup>60,61</sup>, which combine the systems presented here and in other works, such as integrating MHs structures and embedding on-board electronics, battery, and actuators (e.g., via POP-UP MEMS)<sup>63,64</sup>. Micro-robotic feet with multiple fingers (e.g., via a ratchet-motion similarly to SpinyBot<sup>60</sup>) and actuators could be built to enable changes in the direction of the MHs to better control the attachment/detachment of hooks to leaves in order to resist external perturbations (e.g., winds). Successful anchoring depends on the number of hooks that actually engage with the leaf surfaces. This aspect is even more relevant in the field, where determining pre-load conditions beforehand is challenging. Models for compliant hook arrays for hook/asperity interaction<sup>61</sup> could thus be investigated, and predictions of load-sharing among hooks<sup>48,49,61</sup> are needed to guide the design of hook array mechanisms for leaf anchoring. If successful, the resulting machines may find applications in natural ecosystems, perhaps even in difficult-to-access high vegetation-covered areas (e.g., in the rainforest) where they could anchor and climb between plants for continuous remote mobile monitoring of wildlife.

## Conclusion

To conclude, our approach highlights the great potential of using plant-inspired anchoring strategies in miniature machines designed for in situ applications on plant leaf surfaces. Our directional attachment system using *G. aparine*-like microhooks allows not only strong and reversible anchoring on different types of leaf surfaces, similarly to the natural counterparts<sup>22</sup>, but also

demonstrates their potential as a multifunctional tool for in situ leaf monitoring, on-leaf ratchet-like motion and molecular delivery to plant vascular tissues. This thus opens several scenarios of applications in precision forestry and agriculture fields by providing a plant-inspired inspired multifunctional technology that could further our understanding of ecosystems and their complex interaction, and preserve their delicate equilibrium.

## Methods

**Plant materials.** *Galium aparine* L. plants were observed while climbing over the neighbouring vegetation in their natural habitats in the area around Pontedera (Pisa, Italy) (Supplementary Fig. 2). In order to test the artificial prototypes, a total of six plant species and nine plant surfaces with different epidermal and mechanical features were investigated. The plant surfaces included (1) smooth surfaces (young and mature *Magnolia grandiflora*, adaxial side); (2) rough surfaces with differently shaped epidermal cells (*Hedera helix*, adaxial side; *Arum italicum*, adaxial side; *Vitis vinifera* L., adaxial side; *Vitis Lambrusca*, adaxial side); (3) rough surfaces with different hair densities (*Rubus caesius* L., adaxial side; *Rubus caesius* L., abaxial side); (4) rough surfaces with waxes (*Vitis Lambrusca*, abaxial side). The plant species were selected based on a screening of *G. aparine*'s natural environment (i.e., Supplementary Fig. 2a–d, respectively, *Arum italicum*, *Rubus caesius*, *Hedera helix*, and *Vitis vinifera*), for comparison (i.e., smooth surface of *M. grandiflora*), or by testing required applications (i.e., *Vitis lambrusca*, for vineyard monitoring and conservation). All plants were collected from natural habitats, except for *Vitis lambrusca* which was purchased from a nursery. Fresh leaves were sampled from the different plant species on the day of the experiments and kept in a closed box in moist conditions to prevent dehydration artefacts.

**Microfabrication of flexible IPS-MHDs.** A 3D model of *Galium aparine*-inspired artificial abaxial hooks was developed in Solidwork®, as described in detail in ref. <sup>33</sup>. The CAD model (STL) was used to directly print hooks on soft Mylar plastic sheets (0.023 mm, polyethylene terephthalate, PET, RS Components, Inc.) using the Nanoscribe Photonic Professional (GT) system (Nanoscribe GmbH) (Supplementary Fig. 4a, part A). For a detailed description of the microfabrication process on flexible substrate, refer to ref. <sup>33</sup>. The microstructures were printed in IPS Nanoscribe GmbH photoresist as an array of 5 by 5 microhooks (25 hooks, area of



the array:  $16 \text{ mm}^2$ ) using a  $\times 25$  immersion objective at a scan speed of  $30 \text{ mm s}^{-1}$  and a laser (femtosecond laser with central wavelength of  $780 \text{ nm}$ , Topica laser source) and  $15 \text{ mW}$  power. The samples were developed for  $30 \text{ min}$  in Propylene Glycol monomethyl ether acetate (PGMEA; Sigma–Aldrich), rinsed with isopropyl alcohol, washed with deionized water, and dried with air.

For the experiments with different densities, hooks of the same size were printed (100%) whereas the distance between two adjacent hook bases (i.e., edge-to-edge of the base circumferences,  $d_x$ ) was changed. These interhook base distances were increased to obtain lower densities ( $49 \text{ hooks cm}^{-2}$ ,  $d_x$  of  $800 \mu\text{m}$ ) and decreased to obtain higher densities ( $352 \text{ hooks cm}^{-2}$ ,  $d_x$  of  $130 \mu\text{m}$ ) (see Supplementary Table 2).

For the experiments with different sizes, hooks were scaled at 50% and 100% with respect to the natural model and were printed in IPS resist as an array of  $5 \times 5$  hooks, as described above. In addition, hooks scaled up to 200% with respect to the natural model were printed in IP-Q resist as an array of  $5 \times 5$  hooks using a  $\times 10$  objective (see Supplementary Table 3 for the geometrical details of the hooks).

**Microfabrication of self-dissolvable i@fluo-MHDs.** A multistep micro-manufacturing strategy was used to produce self-dissolving isomalt@fluorescein MHDs (Supplementary Fig. 4a, part B). First, an array of  $5 \times 5$  hooks at scale 2:1 with respect to the natural model was printed in IP-Q photoresist (Nanoscribe GmbH) on a rigid silicon wafer substrate, employing the Nanoscribe Photonic Professional system. The silicon wafer was treated with plasma (Colibri Plasma RF  $50 \text{ kHz}$ —Gambetti Kenologia) and then the IP-Q photoresist was poured onto the wafer which was then exposed to the laser beam (centre wavelength of  $780 \text{ nm}$ , Topica laser source), using 90% laser power and a scan speed of  $50 \text{ mm s}^{-1}$  (base of the hook) to  $100 \text{ mm s}^{-1}$  (rest of the structure). The samples were developed as described above for IPS-MHDs. For the micromoulding, the printed devices were silanized by a chemical vapor deposition process (i.e., oxygen plasma treatment and 0.3% perfluorodecyltrichlorosilane (PFOTS) in cyclohexane), covered with poly(dimethylsiloxane) (PDMS), and left under vacuum for two days (at  $25 \pm 2 \text{ }^\circ\text{C}$ ). The PDMS mould was then carefully removed and used for the direct casting of the dissolving material (Supplementary Fig. 4, part B1). The dissolving material consisted of pure powdered isomalt (Sapore puro, Torino, Italy), which was heated at  $100 \text{ }^\circ\text{C}$ , mixed with fluorescein dye and transferred to the mould for casting using a dedicated setup for pressurization under heat, to fill the microhooked-shaped cavities. Finally, the self-dissolving i@fluo-MHDs were obtained by gently removing the material from the PDMS mould. For high-throughput fabrication of multiple i@fluo-MHDs, an alternative two-step micromoulding approach was used (Supplementary Fig. 4, part B2). In this case, the PDMS mould was cast with polycaprolactone (PCL) thermoplastic materials, which were heated for  $3 \text{ min}$  at  $200 \text{ }^\circ\text{C}$ , transferred to the PDMS mould, and gently removed to obtain PCL-made MH-based replicas. Nine replicas were then assembled over a 3D printed squared holder, obtaining a master with multiple MH-based replicas. The master was covered with PDMS and left under vacuum for two days to create a mould for multiple casting of dissolving materials.

**Computational modeling.** A finite element computational model was developed to get further quantitative insights into the hooks-leaf system (Supplementary Fig. 13). Penetration/extraction implies topological variations for which computational methods are still being investigated, soft materials fracture is not yet well understood<sup>65</sup> and exhaustive biomechanical data are not currently available. Consequently, we first considered a simplified problem, namely the initial hook extraction (small vertical displacement from the given embedded configuration). Plant tissue was modeled as a composite brick (Supplementary Fig. 13a), with upper and lower epidermis layers (thickness:  $20 \mu\text{m}$ , elastic modulus:  $13 \text{ MPa}$ , density:  $890 \text{ kg/m}^3$ , Poisson ratio: 0.35)<sup>45–47</sup> caging the middle mesophyll layer (thickness:  $200 \mu\text{m}$ , elastic modulus:  $0.8 \text{ MPa}$ , density:  $890 \text{ kg/m}^3$ , Poisson ratio: 0.35)<sup>45–47</sup>. The hook geometries were imported from a CAD file, and material properties (elastic modulus:  $4.6 \text{ GPa}$ , density:  $1200 \text{ kg/m}^3$ , Poisson ratio: 0.35) were taken from the IPS resist datasheet.

In order to investigate the potential effects of the density of the hooks, periodic boundary conditions were imposed on the side faces of the bricks, and the side length of the bricks ( $530 \mu\text{m}$ ) was defined based on the  $7 \times 7$  array configuration (namely the densest one, see Supplementary Table 2). Null displacement was imposed on the lower epidermis bottom face, and a small ( $10 \mu\text{m}$ ) vertical displacement was incrementally imposed on the hook, by adopting a linear elastic approximation. Discretization (based on a tetrahedral unstructured mesh) and contact conditions (by a penalty method) were defined by using the built-in features of the exploited finite element solver (Comsol Multiphysics 5.6, by COMSOL Inc., USA). The results (Supplementary Fig. 13b) prompted us to develop a simplified 2D penetration model, featuring straight spines incrementally engaging along the spine axial direction with the aforementioned composite tissue (Supplementary Fig. 13c). Large displacement from the starting configuration was accounted for by assuming a nonlinear strain, and the preload (vertical force) per spine needed to achieve a given penetration length (thus depth) was determined. The results were postprocessed using Matlab (The Mathworks Inc., USA).

The 3D computational model was then used to investigate the potential effect of the hook size by comparing the microprinted hook (to scale, i.e., 1:1) with a scaled-up (2:1) one, but still considering the initial extraction phase (Supplementary

Fig. 13d; the larger domain therein is compatible with the  $5 \times 5$  hook array considered in the experiments). The results were postprocessed by using Matlab.

**Light microscopy.** A digital optical microscope (Hirox KH-7700) was used to record pictures and videos of natural and artificial samples.

**Electron microscopy.** To preserve the three-dimensional microstructures, freshly cut leaves were chemically fixed in 2.5% glutaraldehyde, dehydrated through a graded series of ethanol dilutions and then treated in a critical point dryer instrument (Autosamdri-931, Tousimis). All biological and artificial samples were mounted onto aluminum stubs and sputter-coated with a  $15 \text{ nm}$  gold layer (Quorum Q150R ES, United Kingdom). Electron microscope images were obtained with an EVO LS10 scanning electron microscope (Zeiss, Germany), or with a FEI Helios Nanolab Dual Beam scanning electron microscope (FEI company, USA).

**Roughness measurements.** The roughness of leaves was measured using a 3D optical profilometry system (Leica DCM 3D, Leica Microsystems). The average roughness ( $R_a$ ) was quantified at  $\times 10$  magnification (area of  $1.27 \times 0.95 \text{ mm}^2$ ) and  $\times 50$  magnification ( $254.64 \times 190.90 \mu\text{m}^2$ ).  $R_a$  is defined as the arithmetic mean deviation of the profile. Three-dimensional isometric rendering of the plant surfaces was obtained using Leica DCM 3D software. For each plant species, the  $R_a$  of leaves was calculated as the mean of fifteen tests for each magnification.

**Nanoindentation.** The nanoindentation experiments on leaves were performed using an iNano indentation system (Nanomechanics, Inc.) and the ‘Dynamic Flat Punch Complex Modulus’ test, which is a common method for biomaterials<sup>44</sup>. A nanoindenter tip with a  $109 \mu\text{m}$  diameter was used for all tests. For each species, nanoindentation experiments were performed on seven fresh cutter leaf samples (area of about  $1 \text{ cm}^2$ ).

**Fluorescence investigations.** To perform fluorescence investigations, the melted isomalt for MH-based dissolvable patches was mixed with 0.1% of 5(6)-Carboxy-fluorescein dye (Sigma–Aldrich). The microfabricated patches were interlocked onto the adaxial surface of *Vitis lambrusca*, and left for  $3 \text{ min}$  before being removed to take pictures or videos. All fluorescence pictures and videos were taken using a Nikon Eclipse Ni-U upright microscope. Image processing of isomalt@fluorescein transport inside plant veins was performed using ImageJ/Fiji software.

**Hook dissolution experiments.** The geometry changes due to single hook dissolution at the tip level were extracted by analyzing the fluorescence microscopy videos in terms of the 2D-projected area ( $\text{mm}^2$ ) of the hook tip and base (downward-oriented) at different times using ImageJ.

**Measurement of detachment, anchoring, and sliding friction forces.** Attachment force was analysed using a custom-built multiaxis measurement platform with dedicated software (VB.NET), which was used to manage the cycles and data acquisition, as detailed in ref. <sup>33</sup> The setup is equipped with (1) two motorized microtranslation stages, including an M-111.1DG for vertical motion and an M-126.CG1 for the horizontal motion, which are both controlled by a C-863 Mercury Servo Controller and produced by Physik Instrumente GmbH; and (2) a six-axis force/torque sensor (Nano17, ATI Industrial Automation).

Three different types of attachment tests were performed to characterize the adhesive behavior of the MH-based patches on leaves, including pull-off, shear locking and sliding friction force tests. For the pull-off and shear-locking force tests, each sample (both MH-based flexible and self-dissolving devices) was fixed on a glass-slide on the bottom plate, and each freshly cut piece of plant leaf was fixed onto a flat custom-built metal support on the top plate immediately before each test to prevent dehydration artefacts. The top plate was lowered by  $0.2 \text{ mm s}^{-1}$  until it reached the fixed preload. For pull-off tests, a horizontal displacement pulled against the direction of the hooks of  $500 \mu\text{m}$  was used to promote the interlocking of hooks with the leaf substrate, after which the top plate was retracted at  $0.5 \text{ mm s}^{-1}$  until the final detachment. The maximum detachment force was considered to be the mean of the maximum force reached before the final detachment over the cycles. For shear-locking tests, a horizontal displacement pulled against the direction of the hooks of  $5 \text{ mm}$  was used to estimate the maximum locking force of the hooks to the leaf substrate, which is considered to be the maximum force peaks of the force-displacement curves. All tests on i@fluo-MHDs were performed immediately after microfabrication, due to the fast reaction of isomalt with environmental humidity which can lead to artefacts. In addition, control dissolvable devices without hooks were tested for comparison. In total, at least five samples were tested for each plant species for both pull-off and shear-locking tests.

For the sliding friction force tests, the friction forces were obtained by pulling the IPS-MHDs against the direction of the hooks onto the different leaves. The flexible samples (fixed onto the top plate of a custom-made metal holder) were brought into contact with the leaf substrates (fixed onto the bottom plate) without a given preload in order to characterize the samples in natural-like *G. aparine* plant

conditions<sup>22</sup>. This kind of characterization is important in low-weight robotic applications, such as MH-based MiniBot. The bottom plate was moved horizontally at  $0.2 \text{ mm s}^{-1}$  for 10 mm. The distance between the holder and the leaf substrates was 2 mm for all friction tests. For each test run, the mean value of five force peaks of force-displacement curves were calculated. In total, seven tests were performed for each plant species. The protocol used was similar to the one used to investigate the friction forces of natural leaves of *Galium aparine*<sup>22</sup>.

**Electronic circuit.** The electronic circuit was fabricated on Kapton substrate and is based on a microcontroller with integrated Bluetooth radio (CYBLE-014008-00 from Infineon/Cypress), one RGBW sensor placed on the top (VEML6040 from Vishay) and two temperature and humidity sensors placed both on the top and bottom (SHT21 from Sensirion AG). The cross response between temperature and humidity is internally managed by the sensor (SHT21 from Sensirion), which calculates the relative humidity compensating with the measured temperature. Data are transmitted to a receiver module (CY8CKIT-042-BLE-A pioneer base-board from Infineon/Cypress) connected to a PC via a USB. The acquisition circuit has two main states. The first is the active state where sensors are powered, and data are read through a I2C interface and transmitted to the receiver board. In the second state, the sensors are turned off and the microcontroller sleeps for a configurable amount of time to save power until the next measurement. In the active state, the overall circuit consumption is an average of  $3.327 \text{ mA}@4.2 \text{ V}$  over 198 ms. In sleep mode, the overall circuit consumption is  $20.4 \mu\text{A}$  for a time that depends on the application. In our tests we configured a 30 s period, which is equivalent to almost 50 days of working time with the 50 mAh LiPo battery assembled.

#### Design, manufacturing, and testing of MH-based origami-assembled sensor.

A 2D CAD origami-like design structure for the MH-based sensor was created in SolidWorks® (Supplementary Fig. 14a, part 1). The hooks were directly printed onto flexible Mylar sheets using a Nanoscribe Photonic Professional (GT) system (see detailed protocol above in the subsection entitled “Microfabrication of MH-based flexible patches”). A dedicated DeScribe program for ad hoc alignment of hooks including an array of  $10 \times 10$  hooks on one side and  $15 \times 3$ ,  $5 \times 5$ ,  $15 \times 3$  hooks on the other, was implemented for the printing (Supplementary Fig. 14a, part 2). The samples developed were then cut in the 2D origami-like design using a professional laser cutter machine equipped with an alignment camera (Beamo, Flux), and then folded into the final structure (Supplementary Fig. 14a, part 3, 4). The electronic circuit (see above: electronic circuit subsection) was then integrated into the folded structure (Supplementary Fig. 14a, part 5, 6). The weight of the fully integrated sensor is 2.6 g. Experiments for the microclimate monitoring of plant leaves were performed on *Vitis lambrusca* adaxial and abaxial surfaces in growth chamber conditions (temperature  $25^\circ\text{C}$ , 60% humidity, 16–8 h light-dark cycle) and outdoor conditions (from 2 to 6.30 pm).

**Design and manufacturing of the crawling MH-based MiniBot.** A  $3 \times 10$  hook pattern was directly printed on a PET sheet (thickness  $23 \mu\text{m}$ ) using the Nanoscribe Photonic Professional (GT) system as described above. A dedicated DeScribe program with ad hoc alignment of hooks including two arrays of  $3 \times 10$  hooks for each foot of the MiniBot was created (Supplementary Fig. 17a). The samples developed were cut using a cutter machine and folded. A multiphase actuator was produced as described in ref. <sup>62</sup> and was glued with silicone glue between the two sides, which were further reinforced by gluing a  $200 \mu\text{m}$  PET sheet ( $10 \times 20 \text{ mm}$ ) on each side. The proof-of-concept demonstration of the crawling capabilities of the MH-based MiniBot was performed on a *Vitis lambrusca* leaf in growth chamber conditions that included continuous leaf motion caused by the growth chamber’s ventilation system. A dedicated setup equipped with a video camera, a thermal camera (FLIR A325sc, FLIR System AB, Sweden) and an NIR laser source (808 nm, maximum output power 500 mW, Roithner Lasertechnik, Vienna) were used for the crawling demonstration and characterization of the robot and actuator (Supplementary Fig. 17b). The thermal camera was controlled by FLIR software (FLIR Research IR Max software) to extract the temperature profiles of the actuators during the ON/OFF laser cycles.

**Statistics.** All experiments were performed at least in quintuplicate, performing five independent experiments on different samples. Error bars in the graphs represent the standard deviation. ANOVA and post-hoc Tukey’s tests at the 99–95% significant level were performed for multiple comparisons when needed.

#### Data availability

The data that support the findings of this study are available from the corresponding authors upon reasonable request.

Received: 22 April 2021; Accepted: 16 September 2021;  
Published online: 07 October 2021

## References

- Cardinale, B. J. et al. Biodiversity loss and its impact on humanity. *Nature* **486**, 59–67 (2012).
- Cardinale, B. J. et al. The functional role of producer diversity in ecosystems. *Am. J. Botany* **98**, 572–592 (2011).
- Pelletier, T. A., Carstens, B. C., Tank, D. C., Sullivan, J. & Espindola, A. Predicting plant conservation priorities on a global scale. *Proc. Natl Acad. Sci. USA* **115**, 13027–13032 (2018).
- Lew, T. T. S. et al. Species-independent analytical tools for next-generation agriculture. *Nat. Plants* **6**, 1408–1417 (2020).
- Giraldo, J. P., Wu, H., Newkirk, G. M. & Kruss, S. Nanobiotechnology approaches for engineering smart plant sensors. *Nat. Nanotechnol.* **14**, 541–553 (2019).
- Zhao, Y. et al. Multifunctional stretchable sensors for continuous monitoring of long-term leaf physiology and microclimate. *ACS Omega* **4**, 9522–9530 (2019).
- Cao, Y., Lim, E., Xu, M., Weng, J. K. & Marelli, B. Precision delivery of multiscale payloads to tissue-specific targets in plants. *Adv. Sci.* **7**, 1903551 (2020).
- Paul, R. et al. Extraction of plant DNA by microneedle patch for rapid detection of plant diseases. *ACS Nano* **13**, 6540–6549 (2019).
- Palazzari, V. et al. in *2015 IEEE 15th Mediterranean Microwave Symposium (MMS)*. 1–4 (2015).
- Atherton, J. J., Rosamond, M. C. & Zeze, D. A. A leaf-mounted thermal sensor for the measurement of water content. *Sens. Actuators A Phys.* **187**, 67–72 (2012).
- Meder, F. et al. Ultraconformable, self-adhering surface electrodes for measuring electrical signals in plants. *Adv. Mater. Technol.* **6**, 2001182 (2021).
- Laschi, C., Mazzolai, B. & Cianchetti, M. Soft robotics: Technologies and systems pushing the boundaries of robot abilities. *Sci. Robot.* **1**, eaah3690 (2016).
- Pena-Francesch, A., Jung, H., Demirel, M. C. & Sitti, M. Biosynthetic self-healing materials for soft machines. *Nat. Mater.* **19**, 1230–1235 (2020).
- Mazzolai, B., Beccai, L. & Mattoli, V. Plants as model in biomimetics and biorobotics: new perspectives. *Front. Bioeng. Biotechnol.* **2**, 2 (2014).
- Fiorello, I., Del Dottore, E., Tramacere, F. & Mazzolai, B. Taking inspiration from climbing plants: methodologies and benchmarks—a review. *Bioinspir. Biomimet.* **15**, 031001 (2020).
- Del Dottore, E., Sadeghi, A., Mondini, A., Mattoli, V. & Mazzolai, B. Toward growing robots: a historical evolution from cellular to plant-inspired robotics. *Front. Robot. AI* **5**, 16 (2018).
- Xia, Z. *Biomimetic Principles and Design of Advanced Engineering Materials* (John Wiley & Sons, 2016).
- Bar-Cohen, Y. Biomimetics—using nature to inspire human innovation. *Bioinspir. Biomimet.* **1**, P1 (2006).
- Sitti, M. Miniature soft robots—road to the clinic. *Nat. Rev. Mater.* **3**, 74 (2018).
- Palagi, S. & Fischer, P. Bioinspired microrobots. *Nat. Rev. Mater.* **3**, 113 (2018).
- Mazzolai, B. & Laschi, C. A vision for future bioinspired and biohybrid robots. *Sci. Robot.* **5**, eaab6893 (2020).
- Bauer, G. et al. Always on the bright side: the climbing mechanism of *Galium aparine*. *Proc. Biol. Sci.* **278**, 2233–2239 (2011).
- Rowe, N. P. & Speck, T. Stem biomechanics, strength of attachment, and developmental plasticity of vines and lianas. *Ecol. Lianas* **1**, 323–341 (2014).
- Burris, J. N., Lenaghan, S. C. & Stewart, C. N. Climbing plants: attachment adaptations and bioinspired innovations. *Plant Cell Rep.* <https://doi.org/10.1007/s00299-017-2240-y> (2017).
- Gallenmüller, F., Feus, A., Fiedler, K. & Speck, T. Rose prickles and Asparagus spines—different hook structures as attachment devices in climbing plants. *PLoS ONE* **10**, e0143850 (2015).
- Chen, Q., Gorb, S. N., Gorb, E. & Pugno, N. Mechanics of plant fruit hooks. *J. R. Soc. Interface* **10**, 20120913 (2013).
- Melzer, B. et al. The attachment strategy of English ivy: a complex mechanism acting on several hierarchical levels. *J. R. Soc. Interface* **7**, 1383–1389 (2010).
- Darwin, C. in *On the Movements and Habits of Climbing Plants*. John Murray, **9**, 1–118 (1865).
- Soffiatti, P. & Rowe, N. P. Mechanical innovations of a climbing cactus: functional insights for a new generation of growing robots. *Front. Robot. AI* **7**, 64 (2020).
- Gorb, E. & Gorb, S. Contact separation force of the fruit burrs in four plant species adapted to dispersal by mechanical interlocking. *Plant Physiol. Biochem.* **40**, 373–381 (2002).
- Niklas, K. J. Climbing plants: attachment and the ascent for light. *Curr. Biol.* **21**, R199–R201 (2011).
- Marino, A., Filipposchi, C., Mattoli, V., Mazzolai, B. & Ciofani, G. Biomimicry at the nanoscale: current research and perspectives of two-photon polymerization. *Nanoscale* **7**, 2841–2850 (2015).

33. Fiorello, I. et al. Micropatterned devices: climbing plant-inspired micropatterned devices for reversible attachment (*Adv. Funct. Mater.* 38/2020). *Adv. Funct. Mater.* **30**, 2070256 (2020).
34. Balmert, S. C. et al. Dissolving undercut microneedle arrays for multicomponent cutaneous vaccination. *J. Control. Release* **317**, 336–346 (2020).
35. Fiorello, I., Meder, F., Tricinci, O., Filippeschi, C. & Mazzolai, B. in *Conference on Biomimetic and Biohybrid Systems*. 122–133 (Springer 2019).
36. Sentko, A. & Willibald-Ettle, I. *Isomalt. Sweeteners and Sugar Alternatives in Food Technology*, Blackwell Publishing Ltd, 243–274 (2012).
37. Koch, K., Bhushan, B. & Barthlott, W. Diversity of structure, morphology and wetting of plant surfaces. *Soft Matter* **4**, 1943–1963 (2008).
38. Wang, S., Ren, L., Liu, Y., Han, Z. & Yang, Y. Mechanical characteristics of typical plant leaves. *J. Bionic Eng.* **7**, 294–300 (2010).
39. Prüm, B., Seidel, R., Bohn, H. F. & Speck, T. Plant surfaces with cuticular folds are slippery for beetles. *J. R. Soc. Interface* **9**, 127–135 (2012).
40. Abbott, J. R. & Zhu, H. 3D optical surface profiler for quantifying leaf surface roughness. *Surface Topogr. Metrol. Properties* **7**, 045016 (2019).
41. Pathan, A., Bond, J. & Gaskin, R. Sample preparation for scanning electron microscopy of plant surfaces—horses for courses. *Micron* **39**, 1049–1061 (2008).
42. Calusi, B., Tramacere, F., Filippeschi, C., Pugno, N. M. & Mazzolai, B. in *Conference on Biomimetic and Biohybrid Systems*. 532–536 (Springer 2017).
43. Herbert, E. G., Oliver, W. C. & Pharr, G. M. Nanoindentation and the Dynamic Characterization of Viscoelastic Solids. *J. Phys. D: Applied Phys.* **41**, 1–9 (2008).
44. Herbert, E., Oliver, W. & Pharr, G. Nanoindentation and the dynamic characterization of viscoelastic solids. *J. Phys. D Appl. Phys.* **41**, 074021 (2008).
45. Pollastrini, M. et al. Influence of different light intensity regimes on leaf features of *Vitis vinifera* L. in ultraviolet radiation filtered condition. *Environ. Exp. Botany* **73**, 108–115 (2011).
46. Onoda, Y., Schieving, F. & Anten, N. P. A novel method of measuring leaf epidermis and mesophyll stiffness shows the ubiquitous nature of the sandwich structure of leaf laminae in broad-leaved angiosperm species. *J. Exp. Botany* **66**, 2487–2499 (2015).
47. Fariñas, M., Álvarez-Arenas, T. G., Sancho-Knapik, D., Peguero-Pina, J. & Gil-Pelegrín, E. in *2012 IEEE International Ultrasonics Symposium*. 1513–1516 (2012).
48. Ruotolo, W., Roig, F. S. & Cutkosky, M. R. Load-sharing in soft and spiny paws for a large climbing robot. *IEEE Robot. Automation Lett.* **4**, 1439–1446 (2019).
49. Sharma, P., Saggiomo, V., Van Der Doef, V., Kamperman, M. & Dijkstra, A. J. Hooked on mushrooms: Preparation and mechanics of a bioinspired soft probabilistic fastener. *Biointerphases* **16**, 011002 (2021).
50. Felton, S. Origami for the everyday. *Nat. Machine Intell.* **1**, 555–556 (2019).
51. Zhakypov, Z., Mori, K., Hosoda, K. & Paik, J. Designing minimal and scalable insect-inspired multi-locomotion millirobots. *Nature* **571**, 381–386 (2019).
52. Fischer, J. et al. Targeted drug delivery in plants: enzyme-responsive lignin nanocarriers for the curative treatment of the worldwide Grapevine Trunk Disease Esca. *Adv. Sci.* **6**, 1802315 (2019).
53. Santana, I., Wu, H., Hu, P. & Giraldo, J. P. Targeted delivery of nanomaterials with chemical cargoes in plants enabled by a biorecognition motif. *Nat. Commun.* **11**, 1–12 (2020).
54. Patil, H., Tiwari, R. V. & Repka, M. A. *11 Encapsulation via Hot-Melt Extrusion*. (2016).
55. Williamson, J. D., Jennings, D. B., Guo, W.-W., Pharr, D. M. & Ehrenshaft, M. Sugar alcohols, salt stress, and fungal resistance: polyols—multifunctional plant protection? *J. Am. Soc. Hortic. Sci.* **127**, 467–473 (2002).
56. Toyota, M. et al. Glutamate triggers long-distance, calcium-based plant defense signaling. *Science* **361**, 1112–1115 (2018).
57. Fiorello, I. et al. Climbing plant-inspired micropatterned devices for reversible attachment. *Adv. Funct. Mater.* **30**, 2003380 (2020).
58. Birkmeyer, P., Gillies, A. G. & Fearing, R. S. in *2011 IEEE/RSJ International Conference on Intelligent Robots and Systems*. 5087–5093 (2011).
59. Asbeck, A. T., Kim, S., McClung, A., Parness, A. & Cutkosky, M. R. Climbing walls with microspines. In *IEEE ICRA*. pp. 4315–4317 (2006)
60. Kim, S., Asbeck, A. T., Cutkosky, M. R. & Provancher, W. R. in *ICAR'05. Proceedings, 12th International Conference on Advanced Robotics*. 601–606 (2005, IEEE).
61. Jiang, H., Wang, S. & Cutkosky, M. R. Stochastic models of compliant spine arrays for rough surface grasping. *Int. J. Robot. Res.* **37**, 669–687 (2018).
62. Meder, F., Naselli, G. A., Sadeghi, A. & Mazzolai, B. Remotely light-powered soft fluidic actuators based on plasmonic-driven phase transitions in elastic constraint. *Adv. Mater.* **31**, 1905671 (2019).
63. Graule, M. et al. Perching and takeoff of a robotic insect on overhangs using switchable electrostatic adhesion. *Science* **352**, 978–982 (2016).
64. Ma, K. Y., Chirarattananon, P., Fuller, S. B. & Wood, R. J. Controlled flight of a biologically inspired, insect-scale robot. *Science* **340**, 603–607 (2013).
65. Zhang, T., Lin, S., Yuk, H. & Zhao, X. Predicting fracture energies and crack-tip fields of soft tough materials. *Extreme Mech. Lett.* **4**, 1–8 (2015).

## Acknowledgements

This work was funded by the European Union's Horizon 2020 Research and Innovation Programme under Grant Agreement No 824074 (GrowBot Project) and by the National Geographic Society (NGS) under Grant Agreement No EC-62190T-19.

## Author contributions

I.F. and B.M. conceived and designed the study. I.F. microfabricated MH-based samples, conducted experiments on all samples, worked on all environmental demonstrators, collected data, performed data analysis, and wrote the manuscript draft. A.M. developed electronic circuit and software for MH-based sensor and contributed to manuscript. F.M. fabricated the light-powered actuator for MH-based robot and contributed to drug delivery and manuscript. E.S. performed computational modeling and contributed to the manuscript. C.F. and I.F. conducted FIB experiments. C.F. trained I.F. in the use of laboratory instruments. O.T. contributed to the development of the correct moulding protocol. B.M. supervised the work and contributed to the manuscript. All the authors read and revise the current version of the manuscript.

## Competing interests

I.F., A.M., F.M. and B.M. have a pending patent application related to microhooks-based devices for precision delivery to plant vascular tissues. The remaining authors declare no competing interests.

## Additional information


**Supplementary information** The online version contains supplementary material available at <https://doi.org/10.1038/s43246-021-00208-0>.

**Correspondence** and requests for materials should be addressed to Isabella Fiorello or Barbara Mazzolai.

**Peer review information** *Communications Materials* thanks the anonymous reviewers for their contribution to the peer review of this work. Primary Handling Editor: John Plummer. Peer reviewer reports are available.

**Reprints and permission information** is available at <http://www.nature.com/reprints>

**Publisher's note** Springer Nature remains neutral with regard to jurisdictional claims in published maps and institutional affiliations.

 **Open Access** This article is licensed under a Creative Commons Attribution 4.0 International License, which permits use, sharing, adaptation, distribution and reproduction in any medium or format, as long as you give appropriate credit to the original author(s) and the source, provide a link to the Creative Commons license, and indicate if changes were made. The images or other third party material in this article are included in the article's Creative Commons license, unless indicated otherwise in a credit line to the material. If material is not included in the article's Creative Commons license and your intended use is not permitted by statutory regulation or exceeds the permitted use, you will need to obtain permission directly from the copyright holder. To view a copy of this license, visit <http://creativecommons.org/licenses/by/4.0/>.

© The Author(s) 2021